International Journal of Petroleum and Gas Engineering ISSN 5675-0715 Vol. 3 (12), pp. 001-019, December, 2016. Available online at www.internationalscholarsjournals.org © International Scholars Journals

Full Length Research Paper

Filter cake formation on the vertical well at high temperature and high pressure: Computational fluid dynamics modeling and simulations

Mohd. A. Kabir and Isaac K. Gamwo*

United States Department of Energy, National Energy Technology Laboratory, Pittsburgh, PA 15236-0940, USA.

Accepted 19 July, 2016

Oil and gas wells are generally drilled with the intention of forming a filter cake on the wellbore walls to primarily reduce the large losses of drilling fluid into the surrounding formation. Unfortunately, formation conditions are frequently encountered that may result in unacceptable losses of drilling fluid into the surrounding formation despite the type of drilling fluid employed and filter cake created. It is extremely important to optimize filter cake thickness as very thick filter cake can cause stuck pipe and other drilling problems. The focus of this research is to use a computational fluid dynamics (CFD) technique to numerically simulate filter cake formation on the vertical wellbore wall at high-pressure (25,500 psi or 175.8 MPa) and temperature (170°C) conditions. Here, the drilling fluids were treated as a two-phase system of solid particulates suspended in a non-Newtonian fluid. Drilling process simulations were performed for drilling fluid with two particle sizes, 45- and 7- µm, under extreme drilling conditions of high pressure and temperature. The comparison of both scenarios clearly shows that the drilling fluid with larger particles (45 µm) forms thicker filter cake compared to drilling fluids with smaller particles (7 µm). We have further used FLUENT CFD code to successfully simulate filter cake formation on the wellbore wall at moderate pressure (2,000 psi or 13.8 MPa) and temperature (30°C) conditions with drilling fluid of 45 µm particles. The results for axisymmetric and planar wellbore show that the cake formed during extreme drilling processes is thicker than that formed for shallow drilling processes. Filter cake formed on the vertical wellbore wall is nonuniform for both extreme and shallow drilling process.

Key words: Filter cake, two-phase flow, computational fluid dynamics (CFD), deep drilling.

INTRODUCTION

Recently, filter cake formation on the walls of vertical wellbore at extreme pressure and temperature (up to 25,500 psi or 175.8 MPa and 170°C) has attracted the attention of multiphase fluid researchers due to filter cake's crucial role in reducing drilling fluid losses in oil and gas drilling operations (Delhommer, 1987). Filter cake builds up on the wellbore walls in a mechanism similar to soil consolidation during drilling processes, where overbalance pressure forces drilling fluid into the rock formation and leaves solid particles on the walls in the form of a filter cake (Cerasi, 2001).

*Corresponding author. E-mail: gamwo@netl.doe.gov. Tel: +1 412 386 6537. Fax: + 1 412 386 5920.

During the drilling process, solid particulate multiphase drilling fluids are pumped down into the drilling zone through drilling pipe as shown in Figure 1. Modern drilling fluids used in oil production processes are carefully engineered slurries designed to perform several tasks. Among others, the drilling fluids or slurries function to (a) reduce friction and wear on the drilling bit, (b) transport the drilled solids, (c) maintain a favorable pressure difference between the wellbore and the rock formation, (d) cool down the cutters to maintain the temperature below the critical temperature at which cutter properties such as strength and hardness start to change, and (e) generate a filter cake on the wellbore wall to minimize incursion of drilling fluids into the formation (Vaussard, 1986; Maurer, 1997; Spooner, 2004; Ali, 2006; Berry, 2009).

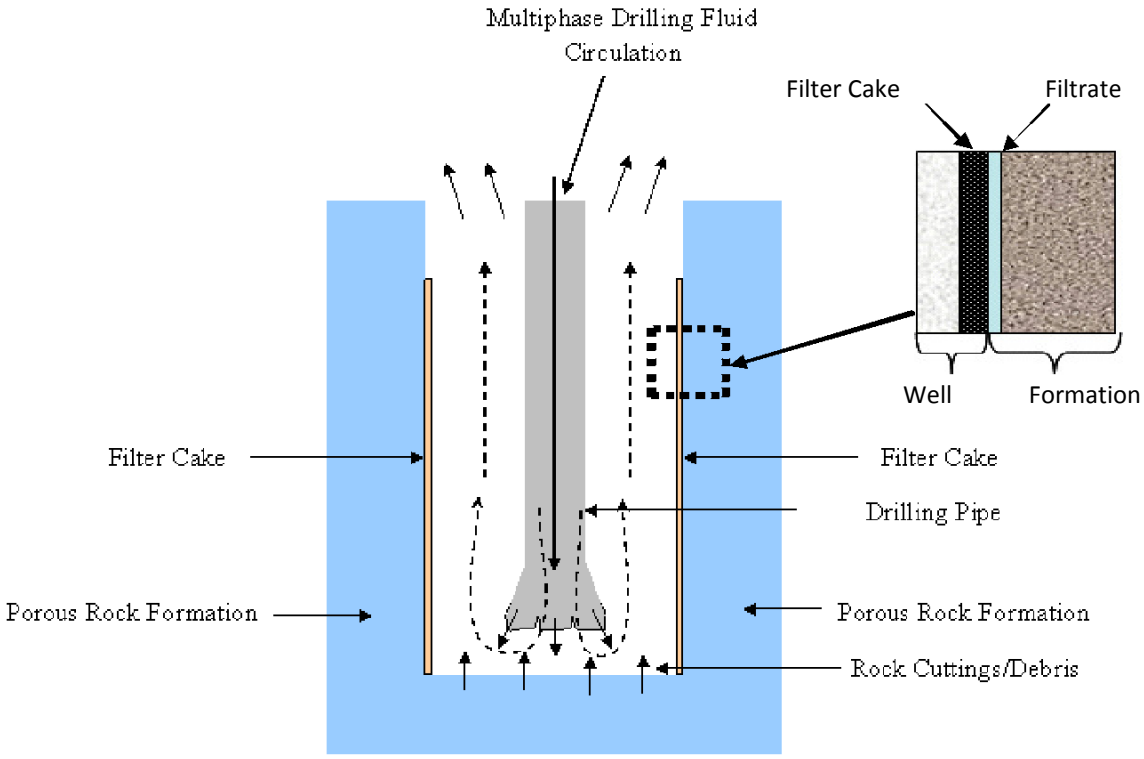

Figure 1. Schematic diagram of drilling fluid circulation in the drilling zone.

The ability to optimize filter cake characteristics is extremely useful (Fisher, 2008). Most wells are drilled with the intention of forming a filter cake of varying thickness on the sides of the borehole. The presence of a filter cake is beneficial since it reduces fluid loss and damage to the formation. However, if the cake is too thick, the effective diameter of the hole is reduced and problems may arise, such as excessive torque when rotating the drill string and excessive drag when pulling it. Thick cakes also contribute to high swab, a decrease in wellbore pressure during the movement of drill strings up the wellbore. Such pressure reduction, if significant, may lead to premature reservoir fluids flowing into the wellbore and towards the surface. Thick cakes may also contribute to sudden increase in pressure (surge pressure) when drill strings or casing is rapidly run into a wellbore, which may be great enough to create lost of drilling fluid circulation.

Earlier research on the filtration (Klotz, 1954; Outmans, 1963; Peden, 1982; Vaussard, 1986; Vaussard, 1986; Delhommer, 1987; Fordham, 1988; Sherwood, 1991) of drilling fluids has suggested that temperature, pressure, hydraulic shear rate, and formation permeability all influence the filtration process. However, the influence of individual factors and their interdependencies remains unclear (Fisher, 2008).

Formation conditions are frequently encountered that may result in unacceptable losses of drilling fluid to the surrounding formation despite the type of drilling fluid employed and filter cake created. The filter cake forms permeable zones in the wellbore wall, which can cause stuck pipe and other drilling problems as well (Delhommer, 1987).

Literature review (Klotz, 1954; Maurer, 1997; Cerasi, 2001; Ali, 2006; Fisher, 2008) shows that very little research has been carried out on filter cake formation during deep drilling. However, limited reports and numerical research do exist on filter cake for shallow-wellbore drilling, although these sources lack detailed information on filter cake formations (Klotz, 1954; Delhommer, 1987; Maurer, 1997; Ali, 2006; Fisher, 2008).

Literature review further reveals that no filter cake formation modeling has yet been performed for deep drilling conditions under high temperature and high pressure. Most of the previous research has been carried out with Newtonian, single phase, and isothermal conditions for shallow drilling process. Hence, we have included the following features in our filter cake formation modeling:

1. CFD simulation of filter cake formation for deep (4 to 5 miles) drilling conditions at high temperature and high pressure.
2. Drilling fluids treated as multiphase non-Newtonian fluid, where solid particulates are suspended in a non-Newtonian fluid phase; the non-Newtonian phase was modeled with power law.

3. Energy equations solved in this numerical modeling and simulation.

In this article, we have used three main interlinked solution aspects to modeling (Fisher, 2008), to simulate the filter cake formation on the vertical wellbore wall in deep (25,000 psi or 172.4 MPa and 170°C) and shallow (2,000 psi or 13.8 MPa and 30°C) drilling processes. The solution aspects used are:

i. Multiphase fluid flow in the pipe and in the annulus between the pipe and the borehole,
ii. Cake formation by deposition of solids from the annulus fluids onto the borehole wall, and
iii. Seepage of mud constituents into the formation during and after cake formation.

The main focus of this research was to investigate the filter cake formation on the vertical well at high temperature and high pressure utilizing computational fluid dynamics (CFD) method tools. The effects of drilling fluid particle sizes on the filter cake thickness were also studied.

MULTIPHASE FLOW AND GOVERNING EQUATIONS

The CFD modeling and simulations involved the solution of Navier-Stokes equations. Hence, detailed equations of multiphase fluids and their relevant theories are also provided here.

The dynamics of solids-in-fluid media have a large effect on various flow phenomena, such as density, viscosity, and pressure. Thus, the hydrodynamics of solids must be modeled correctly (Cornelissena, 2007). The Eulerian approach is preferred over the Lagrangian due to the large volume fraction of solids in the drilling fluid. In the Eulerian approach, fluid and solid phases are treated as interpenetrating continua, and momentum and continuity equations are defined for each phase (FLUENT, 2006). Therefore, the Eulerian-Eulerian multiphase fluid model has been used to simulate fluid flow and filter cake formation in vertical wellbore drilling operations for shallow and deep drilling conditions. The Eulerian model is the most complex of the multiphase models, solving a set of *n* momentum and continuity equations for each phase. Coupling is achieved through the pressure and inter-phase exchange coefficients. The manner in which this coupling is handled depends upon the type of phases involved. For granular flows, properties are obtained by applying kinetic theory. Mass transfer between the phases is negligible and, therefore, ignored here. The momentum equation for the solid phase differs from the equation used for the fluid phase, since the former contains a solid pressure (Ishii, 1975; Jackson, 1997; FLUENT, 2006; Myöhänen, 2006). Lift and virtual mass forces are assumed to be negligible in the momentum equations.

Modeling fluid flow in the annulus

Multiphase equations for modeling the flow of steady, laminar, non-isothermal, incompressible fluid are given thus (Ishii, 1975; Jackson, 1997; FLUENT, 2006; Myöhänen, 2006; Cornelissena, 2007; Gidaspow, 1994, "Jung and Gamwo, 2008").

Conservation of mass

For liquid, $\nabla.(\alpha_l v_l) = 0$ (1)

For solids, $\nabla.(\alpha_s v_s) = 0$ (2)

where α is the volume fraction and subscripts *l* and *s* denote liquid and solid phases, respectively. Moreover, $\alpha_l + \alpha_s = 1$ must be satisfied. v_l and v_s are the velocities of the solid and liquid phases, respectively.

Momentum balance

Liquid phase: The momentum equation for the liquid phase in a solid-liquid system (Ishii, 1975; Jackson, 1997; FLUENT, 2006; Myöhänen, 2006; Cornelissena, 2007) is:

$$\underbrace{\nabla.(\alpha_l \rho_l \vec{v}_l \vec{v}_l)}_{\text{Convective}} = \underbrace{-\alpha_l \nabla p}_{\text{Pressure}} + \underbrace{\nabla.\bar{\tau}_l}_{\text{Stress}} + \underbrace{\alpha_l \rho_l \vec{g}}_{\text{Body Forces}} \underbrace{-K_{sl}(\vec{v}_l - \vec{v}_s)}_{\text{Momentum exchange}} \quad (3)$$

Where ρ_l and ρ_s are the densities of liquid and solid phases, respectively.

To address non-Newtonian behavior of the liquid phase in the multiphase drilling fluid, we have used the power-law model input parameters in the simulation (FLUENT, 2006; Fisher, 2008).

For the fluid, the stress tensor, $\bar{\tau}_l$, is related to the fluid strain rate tensor, $\bar{\dot{\gamma}}_l = \nabla \vec{v}_l + (\nabla \vec{v}_l)^{tr}$, by:

$$\bar{\tau}_l = \alpha_l \mu_l \bar{\dot{\gamma}}_l + \alpha_l \left(\lambda_l - \frac{2}{3}\mu_l\right) \nabla . \vec{v}_l \bar{I} \quad (4)$$

where $\mu_l = k \left|\bar{\dot{\gamma}}_l\right|_{n-1}$ and $\left|\bar{\dot{\gamma}}_l\right|$ is the magnitude of the strain rate tensor defined as $\left|\bar{\dot{\gamma}}\right| = \sqrt{\frac{1}{2}\sum_i \sum_j \dot{\gamma}_{ij} \dot{\gamma}_{ji}}$, and

k and *n* are consistency factor and power-law exponent, respectively (FLUENT, 2006; Fisher, 2008; Hamed, 2009).

Solid phase: The momentum equation for the solid phase in a solid-liquid system (Ishii, 1975; Jackson, 1997; FLUENT, 2006; Myöhänen, 2006; Cornelissena, 2007) is:

$$\nabla.(\alpha_s \rho_s \vec{v}_s \vec{v}_s) = -\alpha_s \nabla p - \nabla p_s + \nabla.\bar{\tau}_s + \alpha_s \rho_s \vec{g} + \sum_{l=1}^{n} (K_{ls}(\vec{v}_l - \vec{v}_s)) \quad (5)$$

Solid pressure

The solids pressure, p_s, stress, $\bar{\tau}_s$ and viscosity, α_s are determined by particle fluctuations and the kinetic energy associated to these fluctuations, granular temperature Θ. The stress-strain relationship for the solid phase *s* is:

$$\bar{\tau}_s = \alpha_s \mu_s (\nabla \vec{v}_s + \nabla \vec{v}_s^T) + \alpha_s \left(\lambda_s - \frac{2}{3}\mu_s\right) \nabla \cdot \vec{v}_s \bar{I} \quad (6)$$

Shear stress, bulk viscosity and unit tensor

$$\bar{\dot{\gamma}}_s = \frac{1}{2}(\nabla \vec{v}_s + (\nabla \vec{v}_s)^T)$$

Where solid strain rate tensor $\bar{\dot{\gamma}}_s$.

Interaction forces are considered here to account for the effects of other phases and are reduced to zero for single phase flow (FLUENT, 2006; Cornelissena, 2007). The momentum exchanges coefficients are indistinguishable ($K_{ls} = K_{sl}$):

$$K_{sl} = \frac{\alpha_s \rho_s f}{\tau_s^p} \quad (7)$$

This function and coefficients are suitable for drilling process modeling where recirculating multiphase fluids contain high solid fraction.

Here, τ_s^p is the particulate relaxation time and f is the model-dependent drag function. The relaxation time is expressed as:

$$\tau_s^p = \frac{\rho_s d_s^2}{18 \mu_l} \quad (8)$$

where d_s is the solid particle diameter.

While the Syamlal-O'Brien drag function f (FLUENT, 2006; Cornelissena, 2007) is used:

$$f = \frac{C_D Re_s \alpha_l}{24 v_{r,s}^2} \quad (9)$$

The relative Reynolds number Re_s can be written as follows (FLUENT, 2006; Cornelissena, 2007):

$$Re_s = \frac{\rho_l d_s |\vec{v}_s - \vec{v}_l|}{\mu_l} \quad (10)$$

The drag function *f* includes a drag coefficient C_D and the relative Reynolds number Re_s; however, the drag function differs among the exchange-coefficient models. For the drilling process, multiphase drilling fluid with a high solid fraction continuously cycles through the drill assembly and carry away debris produced by the drilling process.

In the Syamlal-O'Brien model, the drag function of Dalla Valle is used (FLUENT, 2006; Cornelissena, 2007), where $v_{r,s}$ is the terminal velocity correlation:

$$C_D = \left(0.63 + \frac{4.8}{\sqrt{Re_s / v_{r,s}}}\right)^2 \quad (11)$$

The terminal velocity correlation $v_{r,s}$ for solid phase has the following form:

$$v_{r,s} = 0.5\left(A - 0.06 Re_s + \sqrt{(0.06 Re_s)^2 + 0.12 Re_s (2B - A) + A^2}\right) \quad (12)$$

where $A = \alpha_l^{4.14}$; $B = 0.8\alpha_l^{1.28}$, $\alpha_l \leq 0.85$; $B = \alpha_l^{2.65}$, $\alpha_l > 0.85$

This correlation is based on measurements of terminal velocities of particles in fluidized or settling bed where high solid volume fractions similar to solid volume

fractions in drilling fluids are encountered.

The solid pressure P_S is composed of a kinetic term (first term), a particle collisions term (second terms) and a friction term (3rd term) (FLUENT, 2006; Cornelissena, 2007):

$$P_{sss} = \alpha_s \rho_s \Theta_s + 2\rho_s (1+e_{ss}) \alpha_s^2 g_{0,ss} \Theta_s + F_{sr} \frac{(\alpha_s - \alpha_{s,\min})^n}{(\alpha_{s,\max} - \alpha_s)^p} \quad (13)$$

Both kinetic and collision terms are dependent on the granular temperature Θ . The term e_{ss} is the particle – particle coefficient of restitution (taken here to be e_{ss} = 0.9 - this choice is consistent with literature value under similar simulation conditions) where $g_{0,}$ is the radial distribution function. This is a correction factor (the non-dimensional distance between spheres) that modifies the probability of collisions between particles when the granular phase becomes dense. The friction is included in this study since the solid volume fraction is relatively high, which may give rise to friction. In this work, the friction pressure is modeled using the semi-empirical model proposed by Johnson et al. (1990). $\alpha_{s,min}$ and are the minimum and maximum packing $\alpha_{s,max}$ respectively. $\alpha_{s,min}$, assumed to be 0.5, is the solid concentration when friction stresses becomes important. The values of empirical materials constants F_r, n, and p are taken to be 0.5, 2.0 and 5.0, respectively, following other investigators (Johnson et al., 1990).

Energy equation

To describe the conservation of energy in Eulerian multiphase applications, a separate steady-state enthalpy equation can be written for each phase *q* (liquid or solid) (FLUENT, 2006; Cornelissena, 2007) as follows:

$$\nabla \cdot (\alpha_q \rho_q \vec{u}_q h_q) = (\bar{\tau}_q : \nabla \vec{u}_q) - \nabla \cdot \vec{q}_q + \sum_{p=1}^{n} Q_{pq} \quad (14)$$

where h_q is the specific phase enthalpy, $\vec{q}_q$ is the heat flux, and $\vec{Q}_{pq}$ is the intensity of heat exchange between phases.

Granular temperature

Particulates' viscosities need the specification of the granular temperature for the solid phase. We used a partial differential equation, which was derived from the transport equation by neglecting convection and diffusion. It takes the following form (FLUENT, 2006; Cornelissena, 2007):

$$0 = (-p_s \bar{I} + \bar{\tau}_s) : \nabla \vec{v}_s - \gamma_{\Theta_s} + \varphi_{ls} \quad (15)$$

where $(-p_s \bar{I} + \bar{\tau}_s) : \nabla \vec{v}_s$ is the generation of energy by the solid stress tensor, γ_{Θ_s} is the collisional dissipation of energy, and φ_{ls} is the energy exchange between the fluid and the solid phase.

The collisional dissipation of energy, γ_{Θ_s} , represents the rate of energy dissipation within the solid phase due to collisions between particles. The term is represented by the following expression derived by Lun (1984):

$$\gamma_{\Theta_s} = \frac{12(1-e_{ss}^2) g_{0,ss}}{d_s \sqrt{\pi}} \rho_s \alpha_s^2 \Theta_s^{3/2} \quad (16)$$

The transfer of the kinetic energy of random fluctuations in particle velocity from the solid phase to the liquid phase is represented by φ_{ls} :

$$\varphi_{ls} = -3K_{ls} \Theta_s \quad (17)$$

The radial distribution function, $g_{0,ss}$ is modeled as follows (Ding, 1990; FLUENT, 2006; Cornelissena, 2007):

$$g_{0,ss} = \left[1 - \left(\frac{\alpha_s}{\alpha_{s,\max}}\right)^{1/3}\right]^{-1} \quad (18)$$

where $\alpha_{s,\max}$ is the maximum packing, assumed here to be 0.63 (the symbols are defined in Table 1).

The viscosity for solids stress tensor is the sum of collisional, kinetic, and frictional viscosity parts:

$$\alpha_s = \alpha_{s,col} + \alpha_{s,kin} + \alpha_{s,fr} \quad (19)$$

The collisional part of viscosity is modeled as follows (Ding, 1990; Gidaspow, 1992; FLUENT, 2006; Cornelissena, 2007):

$$\alpha_{s,col} = \frac{4}{5} \alpha_s^2 \rho_s d_s g_{0,ss} (1+e_{ss}) \left(\frac{\Theta_s}{\pi}\right)^{1/2} \quad (20)$$

The kinetic part of viscosity is modeled using the equation of Syamlal (FLUENT, 2006):

Table 1. Definition of symbols.

Symbol	Description	Units
Alphabetic		
C_D	Drag coefficient	Dimensionless
d_s	Solid particle diameter	m
e	Coefficient of restitution	Dimensionless
g	Gravitational acceleration	m/s^2
g_0	Radial distribution function	Dimensionless
K	Interphase exchange coefficient,	Dimensionless
K_p	Porous media permeability	m^2
P	Pressure (Fluid)	Pa
R_e	Relative Reynolds number	Dimensionless
t	Time	s
D_p	Porous media mean particle diameter	m
F_r	Materials constant in eq. 14	
p	Materials constant in eq. 14	
n	Materials constant in eq. 14	
Greek letters		
α	Volume fraction (solid or liquid)	Dimensionless
ρ	Density	kg/m^3
Θ	Granular temperature	m^2/s^2
$\bar{\bar{I}}$	Unit stress tensor	Dimensionless
$\gamma_{\Theta s}$	Collision dissipation of energy	kg/s^3m
$\bar{\bar{I}}_{2D}$	Second invariant of deviatoric stress tensor	Dimensionless
λ	Bulk viscosity	Pa.s
μ	Shear viscosity	Pa.s
$\vec{v}_s$	Solid velocity	m/s
$\vec{v}_l$	Fluid velocity	m/s
v	Seepage velocity	m/s
$\bar{\bar{\tau}}$	Stress tensor	Pa
ε	Porous media void volume fraction	
Subscripts		
col	collision	
fr	friction	
kin	kinetic	
l	liquid phase	
Max, min	Maximum, minimum value	
q	Either liquid or solid phase	
s	Solid phase	

FLUENT (2006), Cornelissena (2007).

$$\mu_{s,kin} = \frac{\alpha_s d_s \rho_s \sqrt{\Theta_s \pi}}{6(3 - e_{ss})} \left[1 + \frac{2}{5}(1 + e_{ss})(3e_{ss} - 1)\right] \alpha_s g_{o,ss} \quad (21)$$

Shear stress includes bulk viscosity, λ_s that in granular flows is related to the particles' resistance to compression and expansion. In Lun et al. (1984), bulk viscosity expression was used in this simulation:

$$\lambda_s = \frac{4}{3}\alpha_s \rho_s d_s g_{o,ss}(1+e_{ss})\left(\frac{\Theta_s}{\pi}\right)^{1/2} \quad (22)$$

When the solids volume fraction is near the packing limit, the friction between particles is important. The friction part of the shear viscosity can be defined using Schaeffer's expression:

$$\mu_{s,fr} = \frac{p_{sfr}\sin\theta}{\sqrt{I_{2D}}} \quad (23)$$

where θ is the angle of internal friction and I_{2D} is the second invariant of the deviatoric stress tensor (FLUENT, 2006).

Porous rock formation model

The multiphase fluid flow through the porous rock is modeled using an extension of Darcy's law for multiphase flow, also referred to as the Ergun equation for laminar flow or the Blake-Kozeny equation. This equation reads:

$$\nabla P = -\frac{\mu}{K_p} v \quad (24)$$

where v is the seepage fluid velocity in the formation and μ the fluid dynamic viscosity. The porous media permeability, K_p , is given below in terms of formation porosity (ε) and the porous media mean pore size (D_p). Here, we set a formation void fraction of 0.2 following Parn-anurak (2003):

$$K_p = \frac{D_p^2 \varepsilon^3}{150(1-\varepsilon)^2} \quad (25)$$

The differential pressure in between the porous media formation and annulus was maintained at 500 psi (3.4 MPa).

Drilling process and filter cake formation

Figure 1 illustrates the drilling fluid circulation process during drilling. Here, particulate multiphase fluid is pumped down into the drilling zone through a drilling pipe where drilling fluid interacts with rock debris. As particulate-laden drilling fluid flows upward to the surface through the annulus in between the walls of the well and the drill string, differential pressure causes filter cake to build up on the porous rock surface as shown in Figure 1.

Since overbalance exists in the annulus, differential pressure forces drilling fluid through the porous rock into the formation and separates the particles on the porous rock surface in the form of filter cake. Fluid that permeates in the porous rock surface is related to the rock resistance, fluid viscosity, and differential pressure. This relationship can be described by Darcy's Law (Fu, 1998; Cerasi, 2001; Parn-anurak, 2003; Fisher, 2008). With time, filter cake will grow on the rock surface; therefore, filter cake itself will also resist fluid permeation into porous rock formations and, hence, fluid permeation will decrease. The resistance from the filter cake can be related to the concentration of mass loading per unit area (kg/m^2) and specific resistance (m/kg). The filter cake builds up to a maximum thickness, which is determined by particle characteristics and fluid shear (Fu, 1998; Fisher, 2008).

Two-dimensional vertical wellbore model

A two-dimensional (2-D) wellbore model was created and meshed with FLUENT- Gambit as shown in Figure 2 (FLUENT, 2006). A symmetry along the central axis was assumed. In this simulation, we zoomed in the drilling zone of a vertical well to capture detailed phenomena occurring in the drilling processes. Hence, the well model is limited to the drilling zone, and the dimensions are 0.24 m wide and 1 m long. To simulate the drilling process, multiphase particulate (α_s = 0.2) drilling fluid was pumped into the main model inlet, and multiphase particulate (α_s = 0.8) rock debris was pushed from the bottom inlet. The main inlet represents drilling fluid pumping in, and the bottom inlet represents rock debris coming from drilling bottom. The solid wall represents the drill string surface. A porous medium with a solid volume fraction of 0.8 next to the drill string represents vertical rock formations on which the filter cake builds up. The pressure and temperature for both inlets are, respectively, 25,500 psi (175.8 MPa) and 170°C for deep drilling conditions, and 2,000 psi (13.8 MPa) and 30°C for shallow drilling conditions. The formation pressure and temperature were maintained at 25,000 psi (172.4 MPa) and 170°C, while the pressure and temperature for shallow drilling conditions were maintained at 1,500 psi (10.3 MPa) and 30°C, respectively, to mimic real-world drilling scenarios. Multiphase particulate non-Newtonian drilling fluids were pumped into the drilling zone where the drilling fluids mingled with rock particles. The particle-laden drilling fluid then flowed upwardly, back to the surface, through the annulus between the walls or sides of the wellbore and the drill string. A variety of drilling fluid types exist, and, as mentioned earlier, the circulation of such fluid functions to, among others things, lubricate the drill bit, remove cuttings from the wellbore as they are produced,

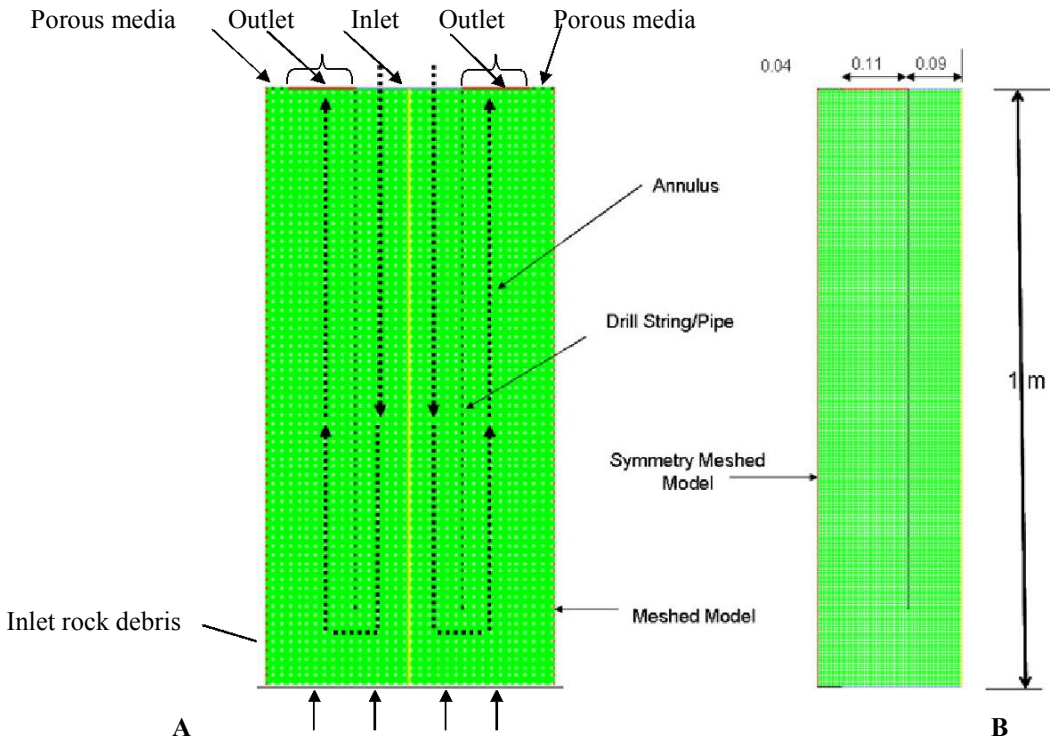

Figure 2. Meshed vertical wellbore model; (a) full-wellbore model; (b) half-wellbore model.

exert hydrostatic pressure on pressurized fluid contained in formations, and seal off the walls of the wellbore so that the fluid is not lost in the permeable subterranean zones (Rogers, 1996).

Initial and boundary conditions

The wellbore was initially filled with multiphase particulate drilling fluid or mud and the bottom portion of the drilling zone was filled with rock debris, as shown in Figure 3. In the model, non-Newtonian power-law fluid properties were given for the liquid phase, and granular properties were given for solid particles. The density of the liquid phase was 999 kg/m^3 with consistency (k) and power-law (n) index of 0.1238 Pa.s^n and 0.67, respectively (Fisher, 2008; Hamed, 2009). The solid phase density was set at 2,350 kg/m^3. Two particle sizes in the fluid were studied: 45 and 7 µm. The domain was discretized with a grid where the flow domain was divided into finite surfaces. As mentioned earlier, axi-symmetry was assumed for modeling the drilling process. There were several trials made (from 5,000 to 11,000 meshes) to eliminate the dependency of the grid size. The half-wellbore model consists of 9,600 numbers of quadrilateral mesh cells with a uniform size of 0.5 x 0.5 cm. The dimension of the porous media formation in the model was 4 x 100 cm, and the porous media formation pressure and temperature were maintained at 25,000 psi (172.4 MPa) and 170°C for deep drilling conditions, whereas the pressure and temperature for shallow drilling conditions were maintained at 1,500 psi (10.3 MPa) and 30°C, respectively.

Model validation for filter cake formation

Our extensive literature review to validate our CFD modeling results revealed very little data available on experimental and numerical filter cake formation on a vertical wall for deep and shallow drilling processes (Sherwood, 1991; Sherwood, 1991; Rogers, 1996; Cerasi, 2001; Usher, 2001; Parn-anurak, 2003; Fisher, 2008; Hamed, 2009). Hence, a single pressure linear filtration process (Figure 4) was chosen to validate our model. Figure 3 shows the initial solid distribution in subsurface vertical wellbore where filter cake forms on the vertical wall, while Figures 4 to 6 show cake formation at the bottom of a laboratory-scale pressure filtration cell. The filter cake formation data were extracted from single pressure filtration CFD simulations and compared with analytically calculated filter cake height to verify the agreement prior to running drilling process simulations.

The simulation was performed for pressure filtration where inlet pressure was kept at 100 kPa. The filtration cell was initially filled with multiphase particulate drilling fluid, and pressure was applied at the top (inlet) with porous media at the bottom (outlet). The applied pressure

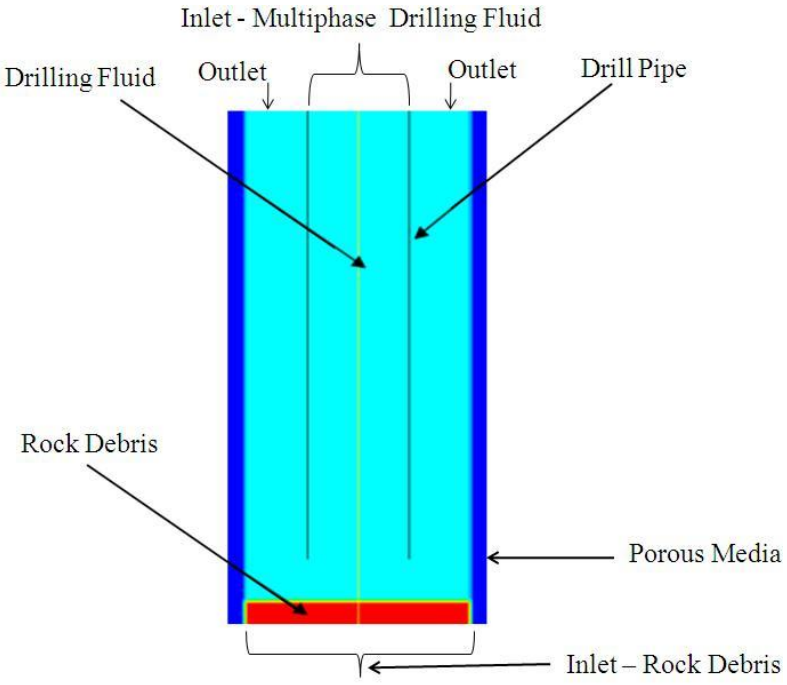

Figure 3. Initial solid volume fraction distribution in the well.

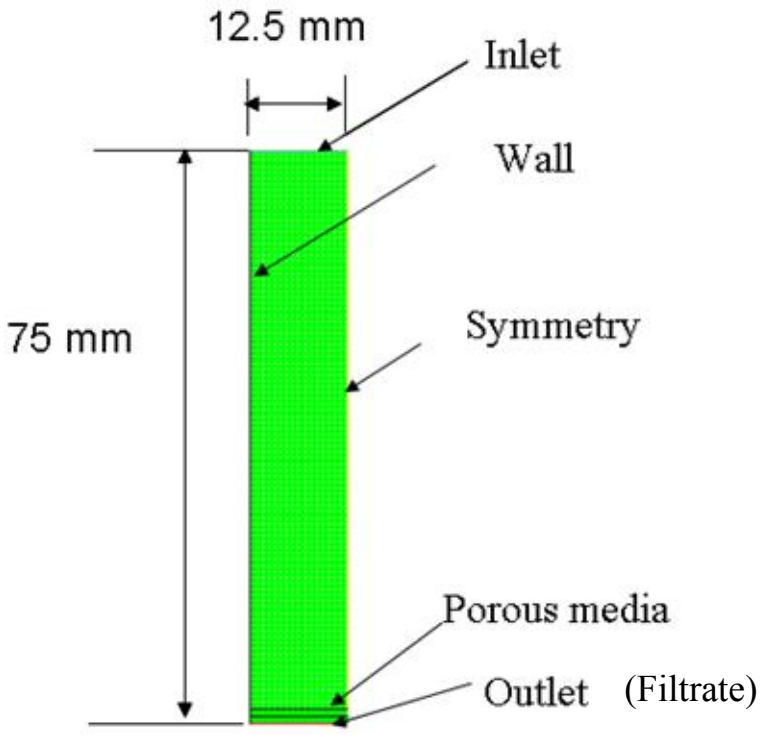

Figure 4. Filtration meshed model created with Gambit (half-filtration cell).

forced fluid through the porous media and separated solid particles in the form of filter cake on the porous me-dia. During filtration, the filter cake that formed reached equilibrium with the applied pressure at the top. Figure 4 shows the symmetry model of the filtration cell. Multi-phase fluid with a solid volume fraction of 0.185 was

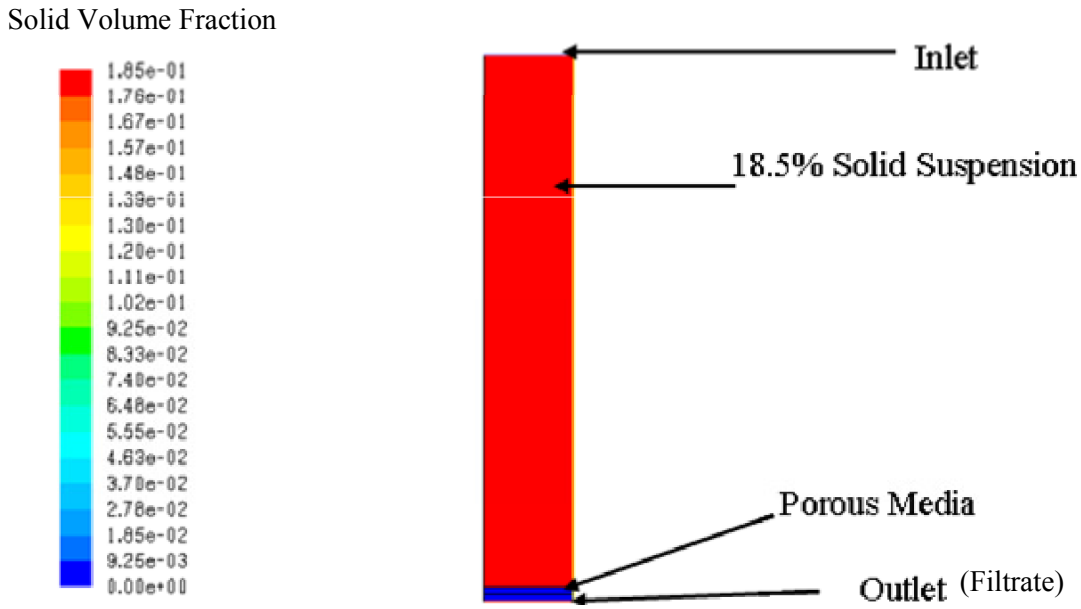

Figure 5. Uniform solid volume fraction of suspension in the filtration model (half-filtration cell).

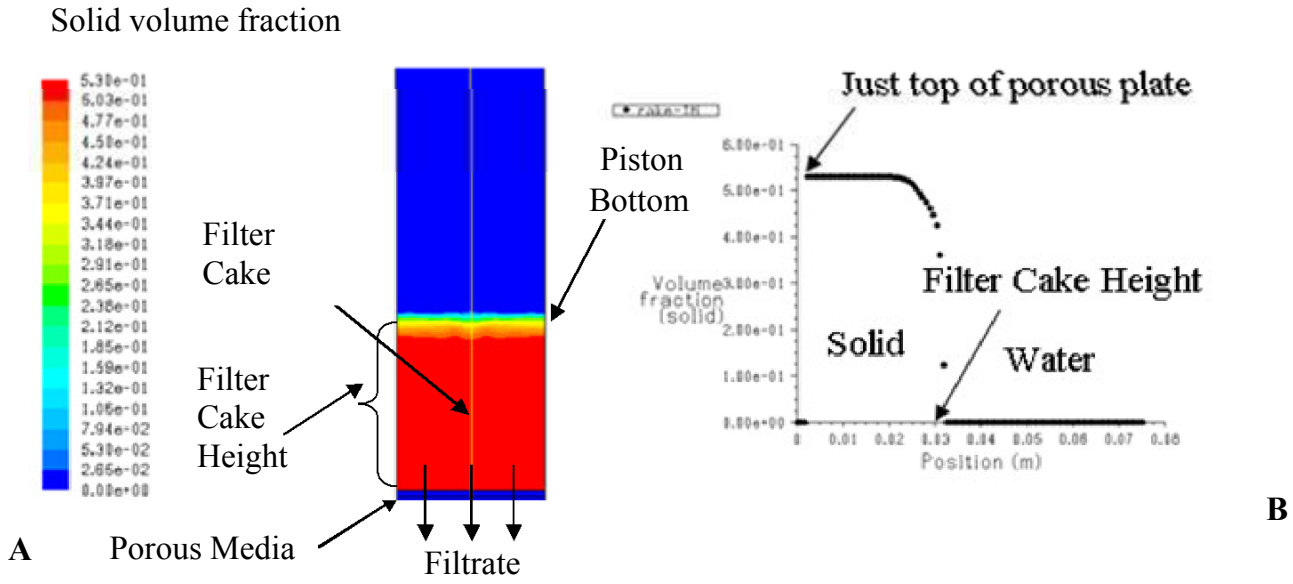

Figure 6. Filter cake formation and profile; a) solid volume fraction distribution; b) solid volume fraction profile at x = 7 mm.

used as an initial condition for simulation, as can be seen in Figure 5. The simulated fluid had the same properties as that of drilling fluid.

Figure 6a shows the simulated filter cake (red) above the porous media. The solid concentration at the bottom increased to about 0.53 due to the filter cake's formation. The interface between the cake and the fluid has a lower solid concentration of around 0.48. This qualitative simulation results are consistent with experimental observations. Figure 6b shows a quantitative solid concentration profile along the vertical axis at radial location x = 7 mm from the left edge. It shows no solid present 30 cm above the porous media.

Similarly, we have extracted the filter cake height from the simulated filtration cell. In order to compare the analytically calculated filter cake height, a theoretical equation was used involving the initial solid volume fraction, α_{so}, equilibrium suspension solid fraction, α_{se}, the initial suspension height, h_o, and equilibrium suspension height, h_e (Usher, 2001). In this equation, the initial solid

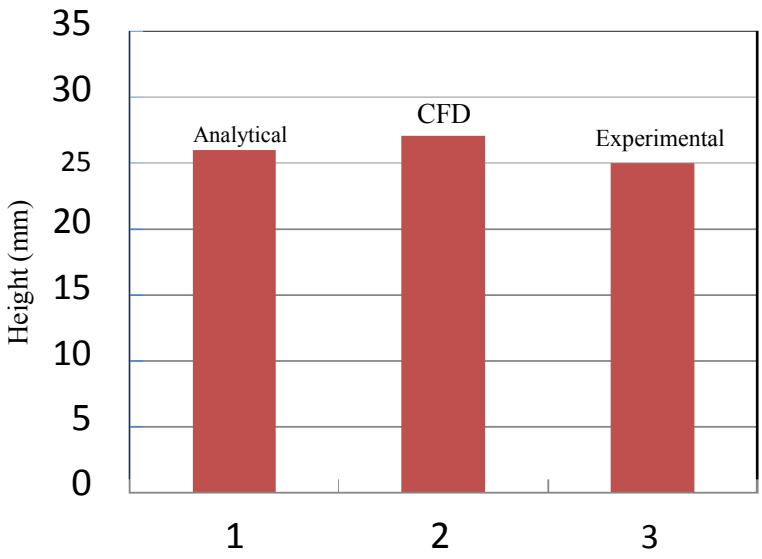

Figure 7. Comparison of filter cake heights.

volume fraction and suspension height of the filtration were α_{so} and $h_{o,}$ respectively. As pressure (P) was applied, filtrate was discharged through the outlet, with the final equilibrium solid volume fraction and the suspension height of α_{se} and h_e, respectively. The conservation of particles mass leads to equation (26) (Usher 2001):

$$h_e = \frac{h_o}{\alpha_{se}} \quad (26)$$

In order to experimentally validate the filter cake thickness, we compared experimental pressure filtration filter cake data of iron ore suspension (Saha, 2009) with CFD simulated and analytically calculated filter cake heights. The details of the iron ore suspension pressure filtration can be found elsewhere (Saha, 2009).

Analytical, experimental, and numerical results of filter cake heights compare reasonably well as shown in Figure 7. The numerical CFD model shows a slightly higher filter cake height compared to analytical results (Figure 7). This is due to the fact that the CFD method accounts for the non-uniform distribution of particles with loosely packed particles near the piston and tightly packed particles near the vicinity of the porous media. The analytical approach assumes uniform distribution of particles throughout the filtration cell.

RESULTS AND DISCUSSION

CFD simulations were performed to simulate filter cake formation in the radial direction on vertical well walls during deep and shallow drilling operations. The initial conditions for both deep and shallow wells are shown in Figure 3 and described earlier. Here, the drilling pipe is filled with drilling fluid and the bottom portion of the well with rock debris/cuttings (Figure 3). Both initial and boundary conditions were similar to conditions found in field drilling operations (Vaussard, 1986; Delhommer, 1987; Sherwood, 1991; Sherwood, 1991; Rogers, 1996; Maurer, 1997; Cerasi, 2001; Usher, 2001; Parn-anurak, 2003; Spooner, 2004; Ali, 2006; Fisher, 2008; Berry, 2009; Hamed, 2009; Wikipedia, 2010). The details of these conditions for shallow and deep drilling simulations are provided in Table 2.

Deep drilling simulation with 45 -µm particles

The deep drilling process was simulated by setting high-pressure (25,500 psi or 175.8 MPa) and high-temperature (170°C) conditions at the inlet and bottom portion of the model. The bottom portion was maintained at the same pressure and temperature as that of inlet. It was assumed that the pressure and temperature varia-tions over a 1- m long model are negligible. Following other researchers (Parn-anurak, 2003), formation poro-sity was assumed to be 0.2. Drilling fluid was pumped down into the drilling zone through the drilling pipe where rock debris mixed with the drilling fluid and was carried away through the annulus. The pressure in the wellbore was maintained higher than the surrounding porous media formation to mimic actual drilling conditions. The differential pressure in the annulus forced the fluid phase through the porous media formation and deposited solid particles in the form of filter cake on the rock surface, as shown in Figure 8; filter cake is defined here as a solid volume fraction above 0.4 at the wall. According to Cerasi and Soga (2001), filter cake grows on the wall in a process similar to soil consolidation, where overbalanced

Table 2. Initial conditions and fluid/formation properties.

Parameter	Shallow well	Deep well
Inlet pressure (drilling fluid/top), psi or MPa	2,000 or 13.8	25,500 or 175.8
Pressure (bottom), psi or MPa	2,000 or 13.8	25,500 or 175.8
Outlet pressure, psi or MPa	1,500 or 10.3	25,000 or 172.4
Formation pressure (porous media), psi or MPa	1,500 or 10.3	25,000 or 172.4
Particle size, µm	45	45 and 7
Formation porosity	0.2	0.2
Temperature, ^{o}C	30	170
Solid fraction (drilling fluid/top)	0.2	0.2
Solid fraction (rock/bottom)	0.8	0.8
Particle density, kg/m^3	2,350	2,350
Fluid density, kg/m^3	999	999

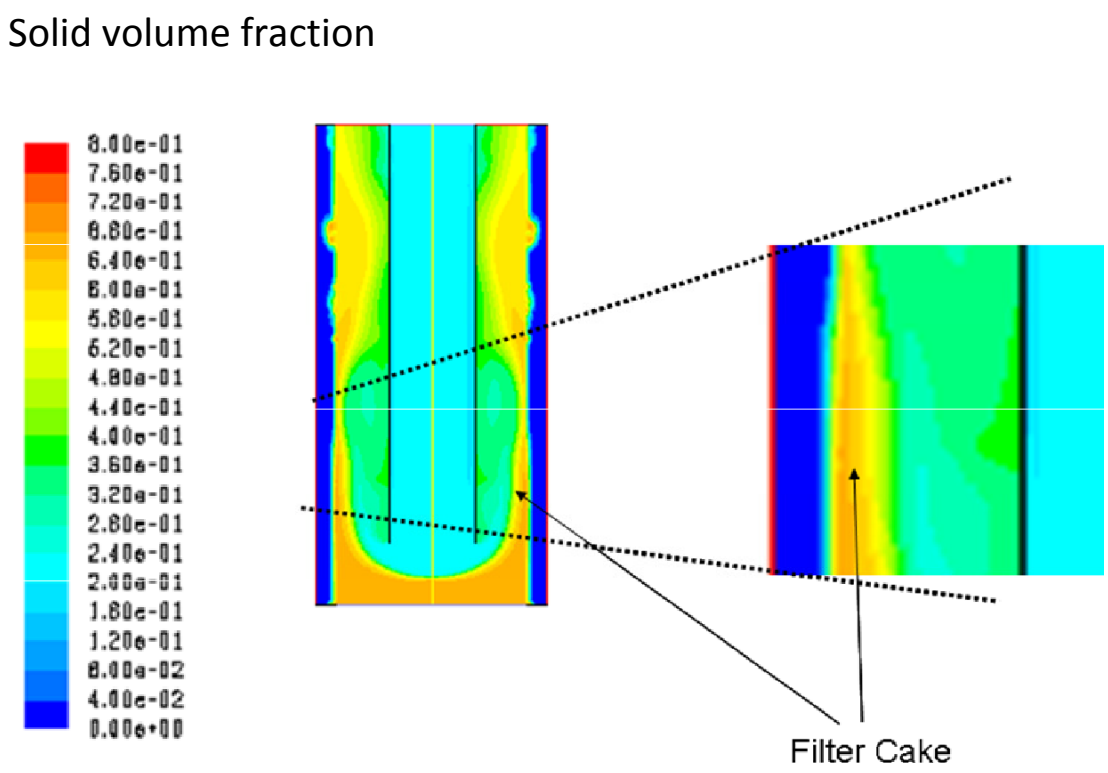

Figure 8. Deep drilling: Filter cake formation on the wellbore wall (solid volume fraction).

pressure will initially force some drilling fluid into the formation, and the solids present in the drilling fluid will clog the pores of the formation and accumulate against the wall under appropriate conditions. As the pressure difference between the wellbore and the formation forces the filter cake to consolidate, the fluid phase (filtrate) invades the formation. The solid particles become more tightly packed, reducing the permeability of the growing cake and, hence, the fluid invasion (Cerasi and Soga, 2001).

The simulated filter cake, as presented in Figure 8, shows that cake forms in non-uniform shapes. This is qualitatively in good agreement with the literature, which reports that non-uniform filter cake forms on the vertical porous rock surface (Sherwood, 1991a, b). Figure 9 shows the solids velocity vector distribution at high-pressure and high-temperature drilling process. Here, the solids maintain nonuniform solid velocities in the annulus, and vortices at the wellbore bottom portion. At the well bottom, the fluid from the pipe encounters drilled solid particles and is forced to drastically change its trajectory. This explains the vortices predicted at the bottom hole.

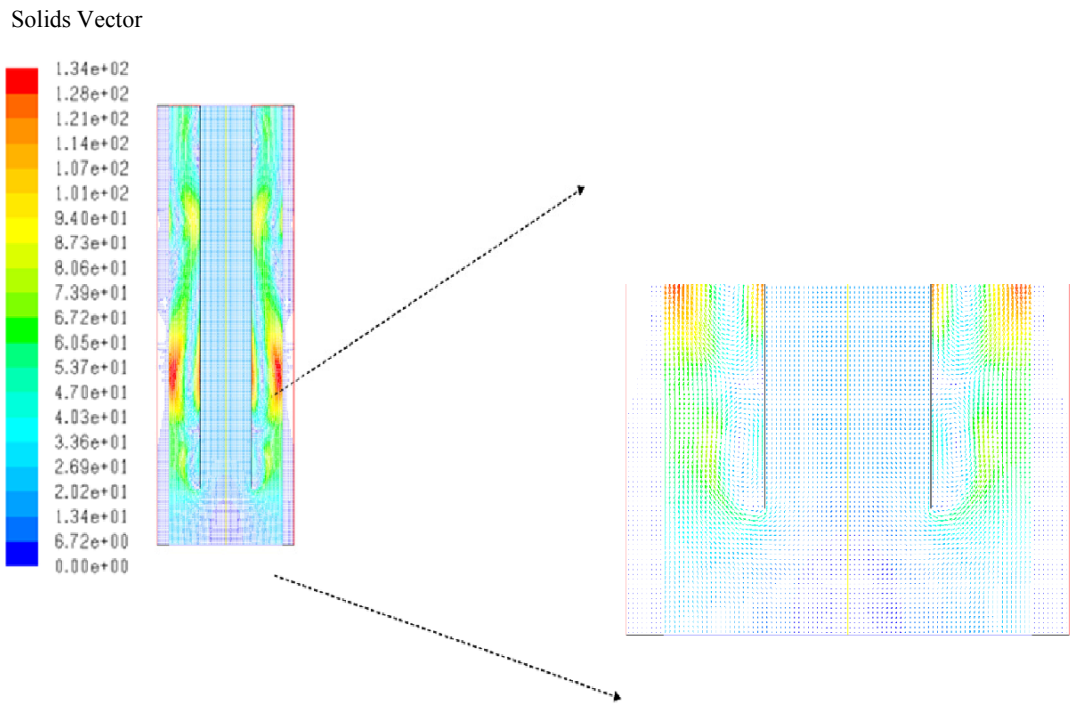

Figure 9. Solids vector distribution.

The vortices also induce nonuniformity in the flow. The ascending fluid loaded with particles rises to the top due to the imposed differential pressure between the hole bottom and the top.

Figure 10a to c show the simulated filter cake in the deep wellbore wall for 45 µm particle in drilling fluid. Figure 10a qualitatively shows filter cake thickness with thinner cake in the lower bottom of the well followed by thicker cake at the upper portion of the well. Figure 10b displays solid volume fractions at different well heights from 0.05 to 0.9 m. Figure 10c exhibits the filter cake thickness extracted from the solid volume fraction graph (Figure 10b). It shows the filter cake thickness versus well heights. The average filter cake thickness varies from 0.023 m near the bottom well to 0.05 m near the top portion. This clearly implies that the simulated filter cake formed on the wellbore wall was non-uniform. This is consistent with experimental observations.

Comparison of deep and shallow drilling simulations

Additionally, nonuniform filter cake was observed in the shallow wellbore, as presented in Figure 11. Figures 11a to c show the simulated filter cake thickness in the shallow wellbore wall with 45 µm particles in the drilling fluid. Figure 11a qualitatively shows the filter cake thickness as thinner in the lower bottom of the well followed by a thicker cake at the upper portion of the well, while Figure 11b shows the solid volume fractions for well heights from 0.05 to 0.9 m.

The filter cake thicknesses were extracted from the solid fraction graph for shallow drilling conditions (Figure 11b) and presented in Figure 11c. It shows the cake thickness over well heights. The average cake thickness next to the bottom was 0.011 m, whereas the average cake thickness near the top was 0.023 m (Figure 11c). The filter cake pattern for shallow drilling conditions was observed to be similar to that of deep drilling conditions.

The non-uniformity of the filter cake thickness in both deep and shallow wells correlates with the magnitude of the vortices in the annulus. It appears large vortices have adverse effects on the filter cake formation with thin filter cake thickness in the bottom region where the vortices intensities are larger and thicker filter cake at the top portion where the vortices intensities are significantly smaller. Hence, vortices' intensities play an important role in the formation of non-uniform filter cake in the well annulus.

Figure 12 compares the simulated filter cake thickness for both deep and shallow drilling conditions. It clearly shows thicker cake for deep drilling conditions. The average cake thickness is 0.04 m for deep drilling processes and 0.0125 m for shallow drilling. Hence, the higher pressure and temperature environment favors thicker cake formation.

Figure 13 compares the solid volume fraction near the well wall for deep and shallow drilling conditions at different heights. It shows higher solid volume fractions for deep drilling. Here, the particles are more consolidated

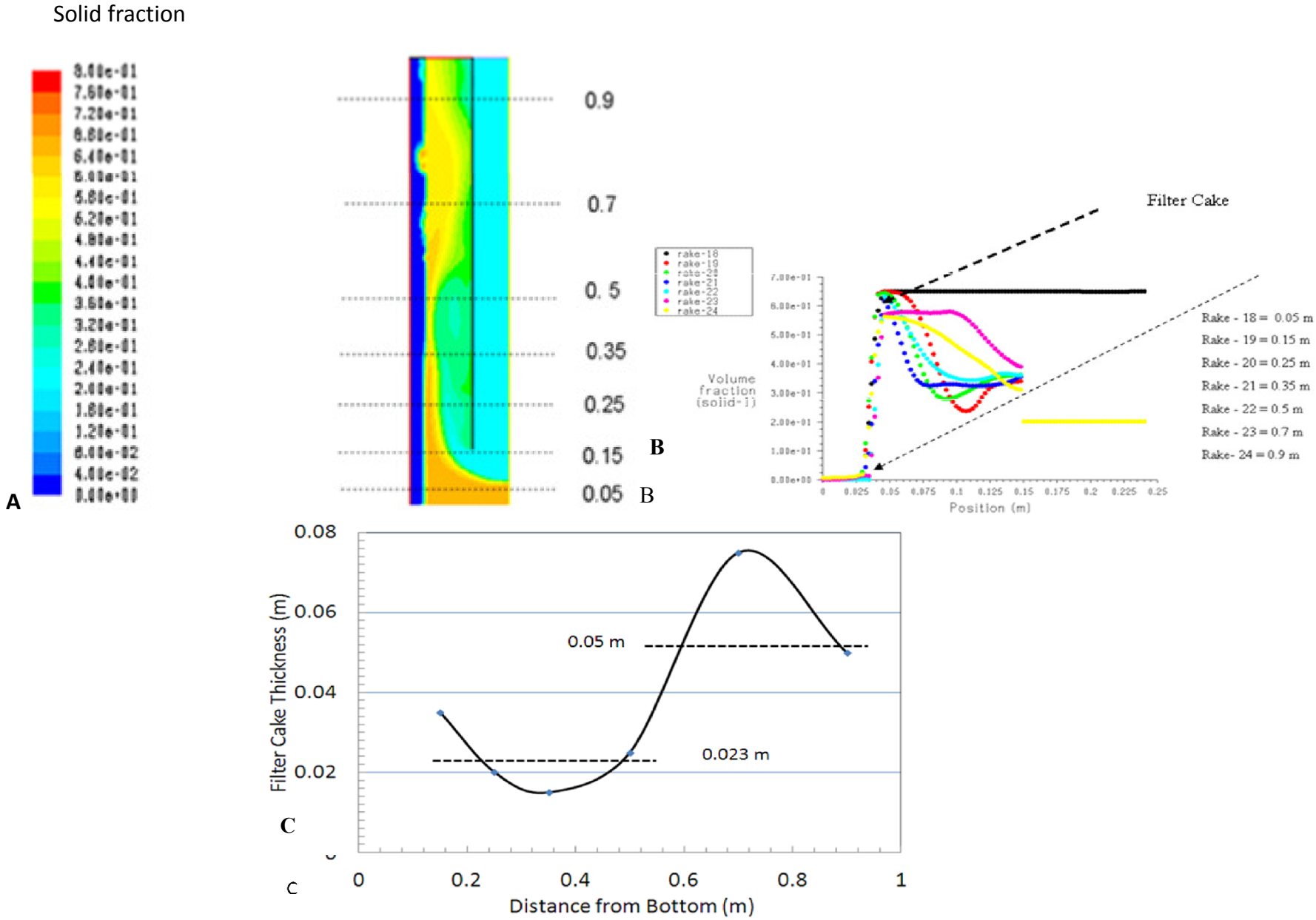

Figure 10c. Deep drilling: Filter cake thickness at different heights of wellbore from bottom; a) qualitative solid volume fraction of well; b) solid volume fraction at different well heights; c) filter cake thickness over well heights.

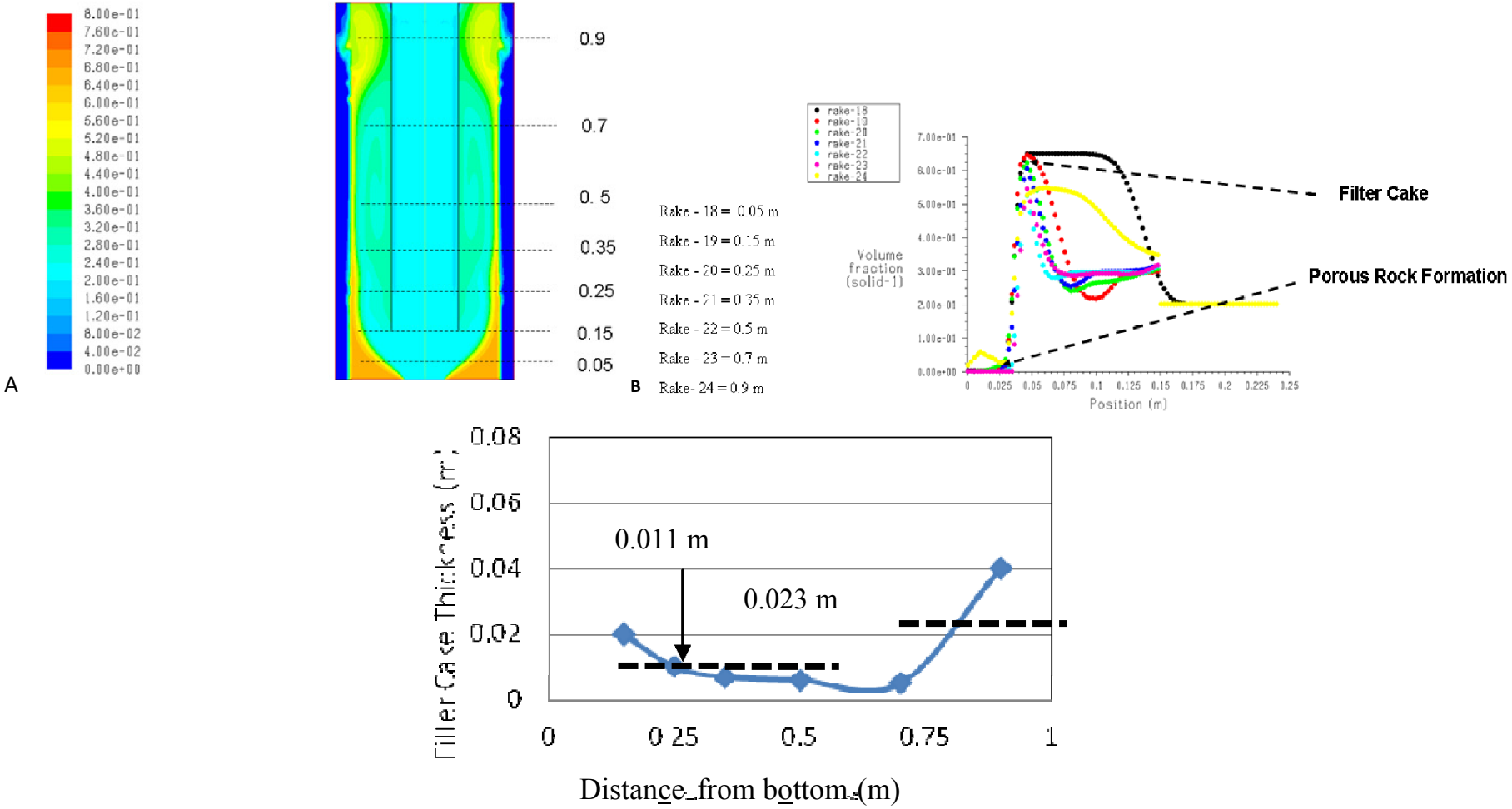

Figure 11a. Shallow drilling: Filter cake thickness at different heights of wellbore from bottom; a) qualitative solid volume fraction of well; b) solid volume fraction at different well heights; c) filter cake thickness over well heights.

due to higher pressure, compared to shallow drilling conditions where the particles remain loosely packed with a lower solid volume fraction. Hence, the higher pressure primarily explains the simulated observations.

Comparison of drilling simulations for 7- and 45- µm particles

Figure 14 shows the simulated filter cake in the deep drilling process with 7-µm particles drilling fluid. Figure 15 compares the filter cake thicknesses for deep drilling with two drilling fluids that differ solely by the particle sizes: 45- and 7- µm in deep drilling conditions. Clearly, the 45 µm drilling fluid leads to a much thicker filter cake, with a

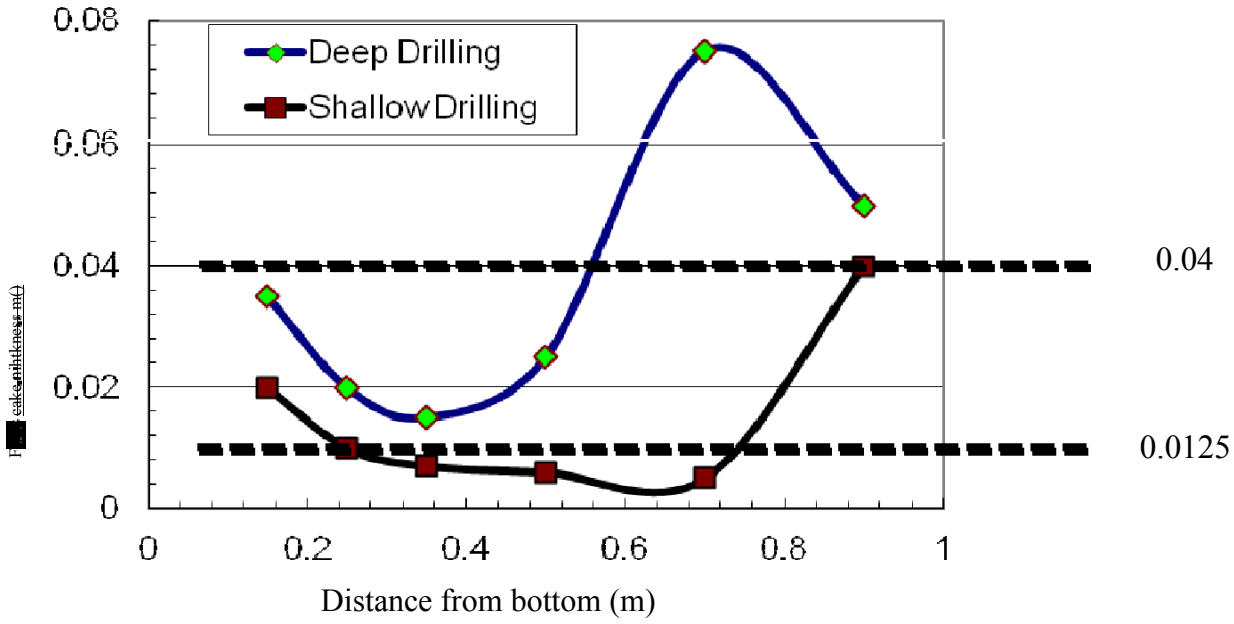

Figure 12. Cake thickness at different heights for deep and shallow drilling.

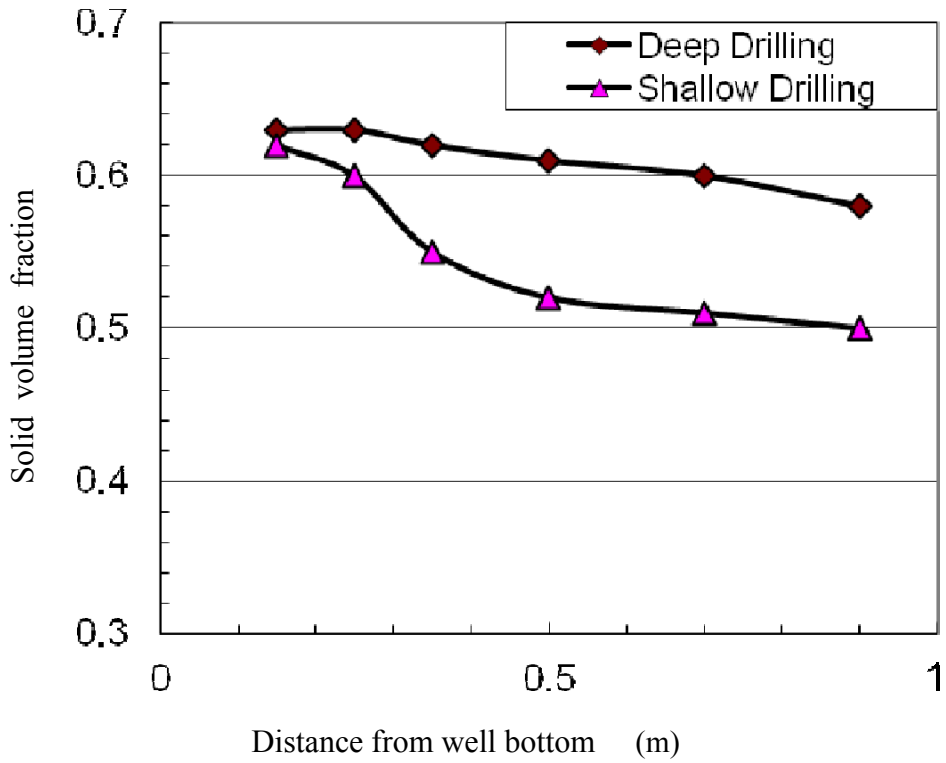

Figure 13. Cake solid volume fraction at different heights for deep and shallow drilling.

average value of 0.04 m compared to 0.008 m for 7- µm drilling fluid. In fact, larger particles formed filter cake five times thicker than smaller particles. Larger particles tend to clog the pores easily, followed by the accumulation of particles on the wall, and this leads to thicker cake formation. Smaller particles tend to travel through the pores easily due to their size; hence, initially they are retained in only a very little amount on the wall to form the filter

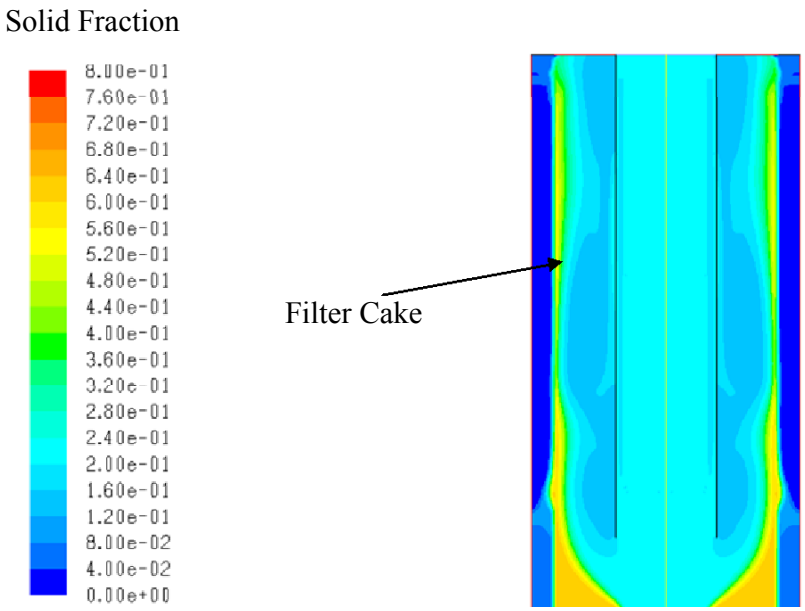

Figure 14. Deep drilling: Qualitative filter cake at different well heights with particle size of 7 µm

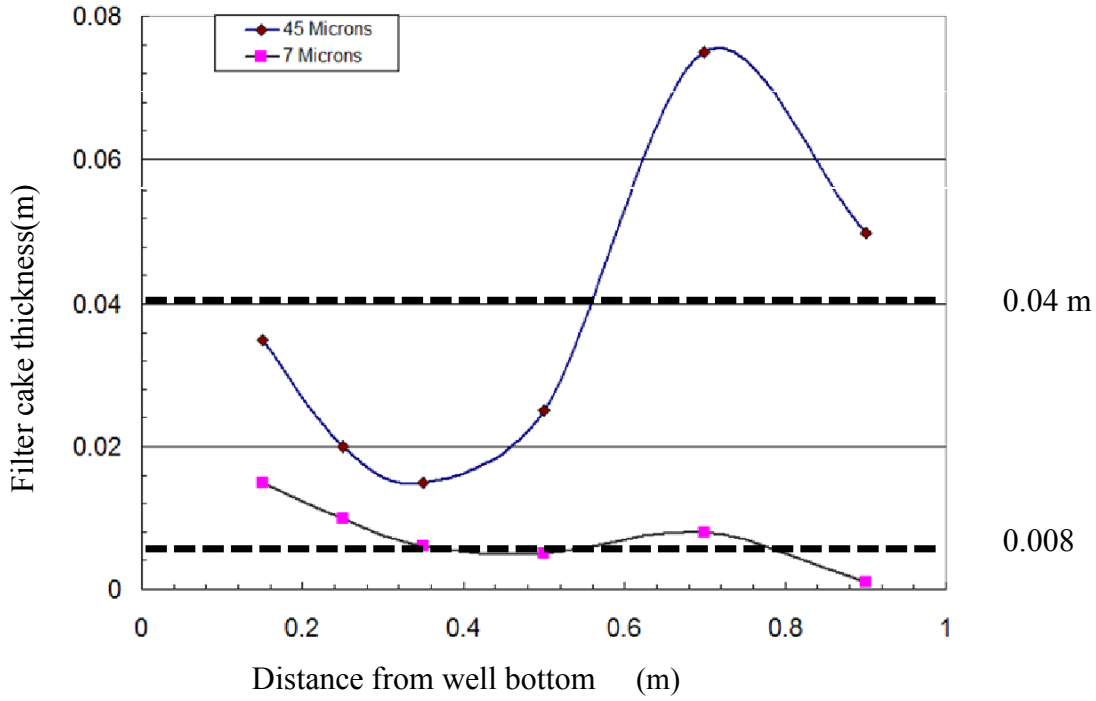

Figure 15. Filter cake thickness at different well heights (high-pressure, high-temperature) for particle sizes of 45 and 7 µm.

cake.

Figure 16 compares the solid volume fraction at x = 0.005 m from the wall for two drilling fluids of different particle sizes of 45- and 7- µm in deep drilling conditions. As expected from our previous simulated results, the solid volume fraction is higher for larger particles. Filter cake thickness optimization based on particle sizes in drilling fluid is important to address in drilling issues arising from very thick cake formation on the wellbore wall.

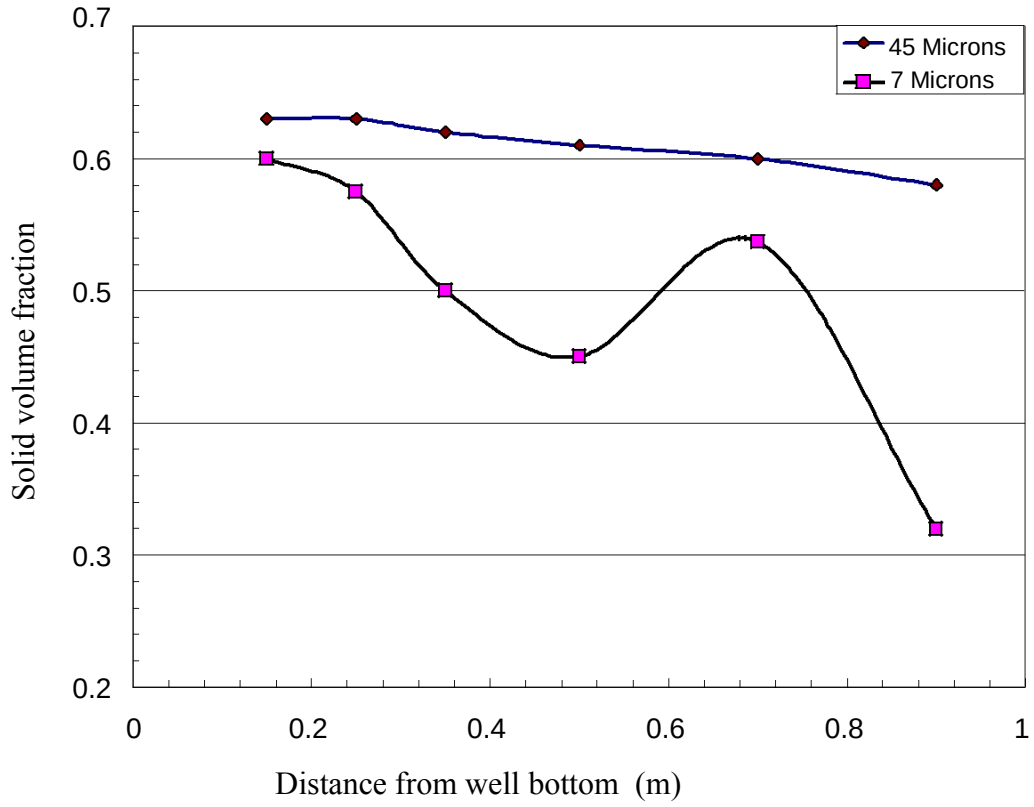

Figure 16. Solid volume fraction of filter cake at different well heights (high-pressure, high-temperature) for particle sizes of 45 and 7 µm.

Conclusion

We have successfully simulated the filter cake formation on the porous rock formation of a vertical wellbore for both deep (5 miles beneath the earth surface) and shallow (0.4 mile) drilling processes using a CFD code FLUENT. The computer-generated filter cakes on porous rock formations are deposited in irregular shapes. This is in agreement with both experimental and analytical claims. The intensity of the vortices observed on the drilling pipe appears to explain the formation of non-uniform filter cake on the well wall. Filter cake thickness and solid volume fractions are higher for extreme drilling processes compared to shallow drilling processes. We believe the higher pressure and temperature surrounding is responsible for thicker cake in the deep drilling process. A parametric study on the effects of drilling fluid particle size clearly shows that larger particles form thicker filter cake compared to smaller particles. Larger particles tend to clog the pores of the porous rock formation while small particles penetrate through the porous rock formation. Hence, it is recommended to use larger particle size in drilling fluids to promote the formation of filter cake, which leads to the prevention of drilling fluid loss through the formation. The model described here may be used to optimize the filter cake thickness during deep and shallow drilling processes for the production of oil and gas.

ACKNOWLEDGEMENTS

This research was supported in part by an appointment to the National Energy Technology Laboratory Research Participation Program, sponsored by the U.S. Department of Energy and administrated by the Oak Ridge Institute for Science and Education. We thank our recent Division Directors J. Brown and J. Thornton as well as our focus area leader G. Guthrie for facilitating this research project.

REFERENCES

AliS (2006). "Reversible drilling-fluid emulsions for improved well performance." Oilfield Review.

Berry JH (2009). "Drilling Fluid Properties & Function, CETCO Drilling Products." from http://www.getco.com.

Cerasi P, Soga K (2001). "Failure modes of drilling fluid filter cake." Geotechnique, 51(9): 777-785.

Cornelissena JT, Toghipour F, Escudiéa R, Ellisa N, Gracea JR (2007). "CFD modeling of a liquid–solid fluidized bed." Chem. Eng. Sci., 62: 6334–6348.

Delhommer HJ, Walker CO (1987). "Method for controlling lost circulation of drilling fluids with hydrocarbon absorbent polymer" US

Patent Number, 4: 633-950.

Ding J, Gidaspow D (1990). “A bubbling fluidization model using kinetic theory of granular flow." J. A.I. Chem. Eng., 36: 523–538.

Ferguson CK, Klotz JA (1954). "Filtration from mud during drilling." Trans AIME, 201: 29-42.

Fisher KA, Wakeman RJ, Chiu TW, Meuric OFJ (2008). "Numerical modeling of cake formation and fluid loss from non-Newtonian mud’s during drilling using eccentric/concentric drill strings with/without rotation." Trans I. Chem. Eng., 78(Part A): 707-714.

FLUENT Inc., (2006) FLUENT 6.3. Lebanon, New Hampshire.

Fordham EJ, Ladva HKJ, Hall C, Baret JF, Sherwood JD (1988). Dynamic filtration of bentonite muds under different flow conditions. 63rd Annual SPE Conference. Houston, Texas SPEFu LF, Dempsey BA (1998). "Modeling the effect of particle size and charge on the structure of the filter cake in ultra-filtration" J. Membrane Sci., 149: 221-240.

Gidaspow D (1994). “Multiphase flow and fluidization: continuum and kinetic theory descriptions" Academic Press, Boston.

Gidaspow D, Bezburuah R, Ding J (1992). Hydrodynamics of circulating fluidized beds, kinetic theory approach In Fluidization VII, Proceedings of the 7th Engineering Foundation Conference on Fluidization.

Hamed SB, Belhadri M (2009). "Rheological properties of biopolymers drilling fluids" SPE, 67: 84-90.

Ishii M (1975). Thermo-fluid dynamic theory of two-phase flow. Collection de la Direction des Etudes et Recherches d'Electricite de France 22. . Eyrolles. Paris. Jackson R (1997). "Locally averaged equations of motion for a mixture of identical spherical particles and a Newtonian fluid." Chem. Eng. Sci., 52(15): 2457-2469.

Johnson PC, Jackson R (1987). "Frictional-collisional constitutive relations for granular materials, with application to plane shearing". J. Fluid Mech., 176: 67-93

Johnson PC, Nott P, Jackson R (1990)."Frictional–collisional equations of motion for participate flows and their application to chutes." J. Fluid Mech., 210:501-535

Jung J, Gamwo IK (2008). "Multiphase CFD-based models for chemical looping combustion process: Fuel reactor modeling". Powder Technol., 183: 401-409.

Lun CKK, Savage SB, Jerey DJ, Chepurniy N (1984). "Kinetic Theories for Granular Flow: Inelastic Particles in Couette Flow and Slightly Inelastic Particles in a General Flow Field." J. Fluid Mech., 140: 223-256.

Maurer Engg. Inc. (1997). "Wellbore thermal simulation model: heory and User's Manual." MAURER ENGINEERING INC. Myöhänen K, Hyppänen T, Kyrki-Rajamäki R (2006). "CFD modeling of fluidized bed systems." SIMS Finland.

Outmans HD (1963). "Mechanics of static and dynamic filtration in the borehole." SPE, 228(236).

Parn-anurak S (2003). "Modeling of fluid filtration and near-wellbore damage along a horizontal well." New Mexico Institute of Mining and Technology. PhDThesis,USA.

Peden JM, Avalos MR, Arthur KG (1982). "The analysis of the dynamic filtration and permeability impairment characteristics of inhibited water based muds." SPE Formation Damage Control Symp. Lafayette.

Rogers HE, Murray DA, Webb ED (1996). "Apparatus and method for removing gelled drilling fluid and filter cake from the side of a wellbore." USA, pp. 5564-500.

Saha H (2009). "Pratical application of filtration theorey to the minerals industry." The University of Melbourne, Australia, PhD Thesis,

Sherwood JD, Meeton GH, Farrow CA, Alderman NJ (1991). "Concentration profile within non-uniform mudcakes." J. Chem. Soc. Far. Trans, 84(4): 611(b).

Sherwood JD, Meeten GH, Farrow CA, Alderman NJ (1991). "Squeeze-film rheometry of non-uniform mudcak." J. Non-Newtonian Fluid Mech., 39: 311-334(a).

Spooner KM, Bilbo D, McNeil B (2004). "The application of high temperature polymer drilling fluid on Smackover operations in Mississippi." AADE-2004 Drilling Fluids Conference. Houston, Texas.

Usher SP, Kretser RG, Scales PJ (2001). "Validation of a new filtration technique for de-waterability characterization." AIChE J., 47(7): 1561-1570.

Vaussard A, Martin M, Konirsch O (1986). "An experimental study of drilling fluids dynamic filtration." SPE, 15412P.

Vaussard A, Martin M, Konirsch O andPatroni JM (1986). "An experimental study of drilling fluids dynamic filtration." 61st Annual Technical Conf. New Orleans, SPE.

Wikipedia (2010). "Oil well," http://en.wikipedia.org/wiki/oil_well.well